


## Article

# Optical and Structural Properties of Composites Based on Poly(urethane) and TiO<sub>2</sub> Nanowires

Malvina Stroe<sup>1</sup>, Teodora Burlanescu<sup>1</sup>, Mirela Paraschiv<sup>1</sup>, Adam Lőrinczi<sup>1</sup>, Elena Matei<sup>1</sup> , Romeo Ciobanu<sup>2,3</sup> and Mihaela Baibarac<sup>1,\*</sup>

<sup>1</sup> National Institute of Materials Physics, P.O. Box MG-7, Bucharest, Atomistilor Street 405A, 077125 Bucharest, Romania

<sup>2</sup> SC All Green SRL, 8 George Cosbuc Str., 700470 Iasi, Romania

<sup>3</sup> Electrical Engineering Faculty, Gheorghe Asachi Technical University of Iasi, Dimitrie Mangeron Bd. 67, 700050 Iasi, Romania

\* Correspondence: barac@infim.ro

**Abstract:** This article's objective is the synthesis of new composites based on thermoplastic polyurethane (TPU) and TiO<sub>2</sub> nanowires (NWs) as free-standing films, highlighting their structural and optical properties. The free-standing TPU–TiO<sub>2</sub> NW films were prepared by a wet chemical method accompanied by a thermal treatment at 100 °C for 1 h, followed by air-drying for 2 h. X-ray diffraction (XRD) studies indicated that the starting commercial TiO<sub>2</sub> NW sample contains TiO<sub>2</sub> tetragonal anatase (A), cubic Ti<sub>0.91</sub>O (C), and orthorhombic Ti<sub>2</sub>O<sub>3</sub> (OR), as well as monoclinic H<sub>2</sub>Ti<sub>3</sub>O<sub>7</sub> (M). In the presence of TPU, an increase in the ratio between the intensities of the diffraction peaks at 43.4° and 48° belonging to the C and A phases of titanium dioxide, respectively, is reported. The increase in the intensity of the peak at 43.4° is explained to be a consequence of the interaction of TiO<sub>2</sub> NWs with TPU, which occurs when the formation of suboxides takes place. The variation in the ratio of the absorbance of the IR bands peaked at 765–771 cm<sup>−1</sup> and 3304–3315 cm<sup>−1</sup> from 4.68 to 4.21 and 3.83 for TPU and the TPU–TiO<sub>2</sub> NW composites, respectively, with TiO<sub>2</sub> NW concentration equal to 2 wt.% and 17 wt.%, indicated a decrease in the higher-order aggregates of TPU with a simultaneous increase in the hydrogen bonds established between the amide groups of TPU and the oxygen atoms of TiO<sub>2</sub> NWs. The decrease in the ratio of the intensity of the Raman lines peaked at 658 cm<sup>−1</sup> and 635 cm<sup>−1</sup>, which were assigned to the vibrational modes E<sub>g</sub> in TiO<sub>2</sub> A and E<sub>g</sub> in H<sub>2</sub>Ti<sub>3</sub>O<sub>7</sub> (I<sub>TiO<sub>2</sub>-A</sub>/I<sub>H<sub>2</sub>Ti<sub>3</sub>O<sub>7</sub></sub>), respectively, from 3.45 in TiO<sub>2</sub> NWs to 0.94–0.96 in the TPU–TiO<sub>2</sub> NW composites, which indicates that the adsorption of TPU onto TiO<sub>2</sub> NWs involves an exchange reaction of TPU in the presence of TiO<sub>2</sub> NWs, followed by the formation of new hydrogen bonds between the -NH- of the amide group and the oxygen atoms of Ti<sub>x</sub>O<sub>2x-mn</sub>, Ti<sub>2</sub>O<sub>3</sub>, and Ti<sub>0.91</sub>O. Photoluminescence (PL) studies highlighted a gradual decrease in the intensity of the TPU emission band, which is situated in the spectral range 380–650 nm, in the presence of TiO<sub>2</sub> NW. After increasing the TiO<sub>2</sub> NW concentration in the TPU–TiO<sub>2</sub> NW composite mass from 0 wt.% to 2 wt.% and 17 wt.%, respectively, a change in the binding angle of the TPU onto the TiO<sub>2</sub> NW surface from 12.6° to 32° and 45.9°, respectively, took place.



**Citation:** Stroe, M.; Burlanescu, T.; Paraschiv, M.; Lőrinczi, A.; Matei, E.; Ciobanu, R.; Baibarac, M. Optical and Structural Properties of Composites Based on Poly(urethane) and TiO<sub>2</sub> Nanowires. *Materials* **2023**, *16*, 1742. <https://doi.org/10.3390/ma16041742>

Academic Editor: Aminul Islam

Received: 15 January 2023

Revised: 17 February 2023

Accepted: 19 February 2023

Published: 20 February 2023

**Keywords:** TiO<sub>2</sub> nanowires; poly(urethane); composites



**Copyright:** © 2023 by the authors. Licensee MDPI, Basel, Switzerland. This article is an open access article distributed under the terms and conditions of the Creative Commons Attribution (CC BY) license (<https://creativecommons.org/licenses/by/4.0/>).

## 1. Introduction

Various conformations of TiO<sub>2</sub> particles, such as nanowires, nanorods, and nanobelts, have been synthesized [1]. The protocols used for the synthesis of TiO<sub>2</sub> particles were: (i) hydrothermal/solvothermal [2]; (ii) sol–gel synthesis [3]; (iii) surfactant-assisted [4]; (iv) microwave-assisted [5]; (v) sonochemical synthesis [6]; (vi) high-temperature pyrolysis [7]; (vii) electrospinning [8]; (viii) chemical/physical vapor deposition [9,10]; (ix) atomic layer deposition [11]; (x) pulsed laser deposition [12]; (xi) suspended molecular template [13]; and (xii) electrochemical deposition [1,14]. That used by Sigma-Aldrich for the synthesis of TiO<sub>2</sub> NWs was the hydrothermal method. Other conformations of TiO<sub>2</sub> particles, such as nanocubes [5], nanospheres [5], nanorods [5], nanowires [15], nanotubes [16],

nanosheets [17], nanobelts [18], etc., were reported. Considerable information concerning the polycrystallinity of TiO<sub>2</sub> was discovered by X-ray diffraction in 2016 [19]. The main crystalline phases reported in the case of TiO<sub>2</sub> nanoparticles were rutile [20], anatase [21], and brookite [22]. The band gap of TiO<sub>2</sub> nanoparticles with a rutile-, anatase-, or brookite-type crystalline phase was of 1.78 eV, 2.04 eV, and 2.2 eV, respectively [23]. One of the most considerable applications of TiO<sub>2</sub> was in the field of photocatalysis [24]. To enhance the photocatalytic properties of TiO<sub>2</sub>, different strategies have been adopted for doping TiO<sub>2</sub> with metals and non-metals, as recently reported by P.S. Basavarajappa et al. [24]. To develop other applications, special attention was paid to the synthesis of composites based on TiO<sub>2</sub> particles and polymers of types such as poly(vinylidene fluoride) [25], polyacrylonitrile [26], polypyrrole–chitosan [27], fluor-polydopamine [28], poly(3-methyl thiophene) [29], poly(3-hexyl thiophene) [30], poly(3,4-ethylenedioxythiophene):poly(2-styrene sulfonate) [31], polyaniline [32], and thermoplastic polyurethane [33]. The main applications of composites based on thermoplastic polyurethane (TPU) and TiO<sub>2</sub> nanoparticles were reported in Li-ion batteries [34], binder for asphalt [35], water filters [36], the adsorption of oils spilled in water [37], and photocatalysis [38]. For such applications, composites containing TiO<sub>2</sub> nanoparticles with anatase- (A) [33,35,39] and rutile-type (R) [40] crystalline phases were used. The synthesis methods used to prepare the TPU–TiO<sub>2</sub> composites included phase inversion [34], mixing in the melting [39], and the wet-spinning process [38]. The most used methods for the characterization of the TPU–TiO<sub>2</sub> composites were X-ray diffraction (XRD) [34], FTIR spectroscopy [34,35,39,40], scanning electron microscopy (SEM) [37,40], and thermogravimetry [38,39]. Cross-linked composites reportedly resulted from the interaction between TPU with TiO<sub>2</sub> nanoparticles and a type-R crystalline phase [40]. Compared with the progress made in the literature, our work was focused on the synthesis of composites based on TPU and TiO<sub>2</sub> nanowires (NWs) and then on highlighting their structural and optical properties by XRD, Raman scattering, FTIR spectroscopy, photoluminescence, scanning electron microscopy (SEM), and energy-dispersive X-ray spectroscopy (EDS). Our motivation for this study was to consider the possibility of using a TPU–TiO<sub>2</sub> NW composite in the field of ventricular catheters, which are currently manufactured from poly(dimethyl)siloxane (PDMS) and polyurethanes (PU) [41,42]. The main disadvantages of these ventricular catheters are protein adsorption, shunt obstruction, and the appearance of infections [41,42]. The interaction of polymers with compounds with increased hydrophilicity and photocatalytic properties, such as TiO<sub>2</sub>, can overcome these inconveniences. Consequently, our aim was the synthesis of TPU–TiO<sub>2</sub> NW composites, highlighting the potential interactions between the two constituents of these composites. Our preliminary results will open new opportunities for optimizing these composites and evaluating their performance in the field of ventricular catheters.

Here, we used XRD to uncover information about the crystalline planes of TiO<sub>2</sub> NWs. We show that the NWs contain tetragonal TiO<sub>2</sub> anatase (A), cubic Ti<sub>0.91</sub>O (C), orthorhombic Ti<sub>2</sub>O<sub>3</sub> (OR), and monoclinic H<sub>2</sub>Ti<sub>3</sub>O<sub>7</sub> (M). To highlight the potential changes in the chemical structure of TPU and TiO<sub>2</sub> NWs, we show the correlated studies by Raman scattering and FTIR spectroscopy. According to our previous study, these characterization methods are valuable tools to highlight the exchange reaction of TPU in the presence of BaTiO<sub>3</sub> nanoparticles [43]. Using scanning electron microscopy (SEM), we show the fibrous structure of the TPU–TiO<sub>2</sub> NW composites. To assess the binding angle of TPU onto the TiO<sub>2</sub> NW surface, we performed anisotropic PL measurements. Our research allows an understanding of TPU's adsorption process onto the TiO<sub>2</sub> NW surface. Recently, we demonstrated that TPU shows, at an excitation wavelength of 350 nm, a photoluminescence (PL) band with maximum at 410 nm [43]. We also analyzed the influence of TiO<sub>2</sub> NWs on TPU PL properties.

## 2. Materials and Methods

### 2.1. Materials

TPU was purchased from the Elastollan-BASF Chemical Company (Cleveland, OH, USA), while TiO<sub>2</sub> NWs and N,N'-dimethyl formamide (DMF, 99.8%) were purchased from Sigma-Aldrich (St. Louis, MO, USA). According to the TiO<sub>2</sub> NWs specification sheet, the diameter and length of the NWs were ~10 nm and ~10 μm.

### 2.2. Synthesis Method of TPU–TiO<sub>2</sub> NW Composites

The free-standing-film TPU–TiO<sub>2</sub> NW composites were prepared by the wet chemistry method as follows: (a) we dissolved 0.5 g TPU in 16 mL DMF under ultrasonication; (b) in each solution of TPU in DMF (0.5 g/16 mL), we added 50 or 100 mg of TiO<sub>2</sub> NW; (c) the dispersion of TiO<sub>2</sub> particles in the TPU solution was performed under ultrasonication for 20 min; (d) the TiO<sub>2</sub> suspensions in the solutions of TPU in DMF were poured into a petri vessel and subjected to a thermal treatment for 1 h at a temperature of 100 °C for DMF evaporation; and (ed) we dried the TPU samples with different TiO<sub>2</sub> concentrations, i.e., 2 wt.% and 17 wt.%, in air for 2 h until the free-standing films' mass remained constant.

The TPU free-standing films were prepared as above without adding the TiO<sub>2</sub> NWs.

Figure 1 shows the schematic synthesis method for TPU–TiO<sub>2</sub> NW composites as free-standing films.

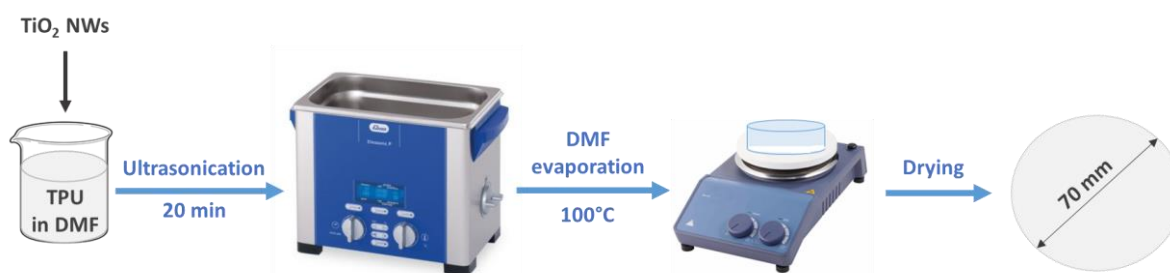


**Figure 1.** Synthesis method for TPU–TiO<sub>2</sub> NW composites as free-standing films.

### 2.3. Methods

#### 2.3.1. X-ray Diffraction Analysis

The XRD patterns of the TiO<sub>2</sub> NWs and TPU–TiO<sub>2</sub> NW composites, which have a TiO<sub>2</sub> NW concentration equal to 2 wt.% and 17 wt.%, respectively, were carried out using a Bruker D8 Advance diffractometer (Bruker, Hamburg, Germany) in Bragg–Brentano geometry, which was equipped with a Cu tube, and which had a Cu K<sub>α</sub>-line of  $\lambda = 1.5406 \text{ \AA}$ .

#### 2.3.2. Fourier-Transform Infrared (FTIR) Spectroscopic Analysis

The IR spectra of TPU and the TPU–TiO<sub>2</sub> NW composites, which had TiO<sub>2</sub> NW concentrations equal to 2 wt.% and 17 wt.%, respectively, were recorded using an FTIR spectrophotometer Vertex 80 model from Bruker (Billerica, MA, USA).

#### 2.3.3. FT-Raman Spectroscopic Analysis

The Raman spectra of TPU and the TPU–TiO<sub>2</sub> NW composites, which have TiO<sub>2</sub> NW concentrations equal to 2 wt.% and 17 wt.%, respectively, were recorded with an FT-Raman spectrophotometer MultiRam model from Bruker at an excitation wavelength of 1064 nm (Ettlingen, Germany).

#### 2.3.4. Photoluminescence Analysis

The photoluminescence (PL) spectra of TPU and the TPU–TiO<sub>2</sub> NW composites, which have TiO<sub>2</sub> NW concentrations equal to 2 wt.% and 17 wt.%, respectively, were recorded with a Fluorolog-3 spectrophotometer FL3-2.2.1 model from Horiba Jobin Yvon (Palaiseau, France).

### 2.3.5. Scanning Electron Microscopy and Energy-Dispersive X-Ray Analysis

Scanning electron microscopy (SEM) and energy-dispersive X-ray (EDS) analysis of TPU and the TPU–TiO<sub>2</sub> NW composites, which have TiO<sub>2</sub> NW concentrations equal to 2 wt.% and 17 wt.%, respectively, were achieved with a Zeiss Gemini 500 field-emission scanning electron microscope and a Zeiss EVO 50 XVP system (Zeiss, Oberkochen, Germany) equipped with a Bruker EDS detector, respectively.

## 3. Results and Discussion

### 3.1. Morphological Properties of TiO<sub>2</sub> NWs and the TPU–TiO<sub>2</sub> Composites

Figure 2 shows the SEM images of TiO<sub>2</sub> NWs, as well as TPU and the TPU–TiO<sub>2</sub> NW composites, which have TiO<sub>2</sub> NW concentrations equal to 2 wt.% and 17 wt.%, respectively.

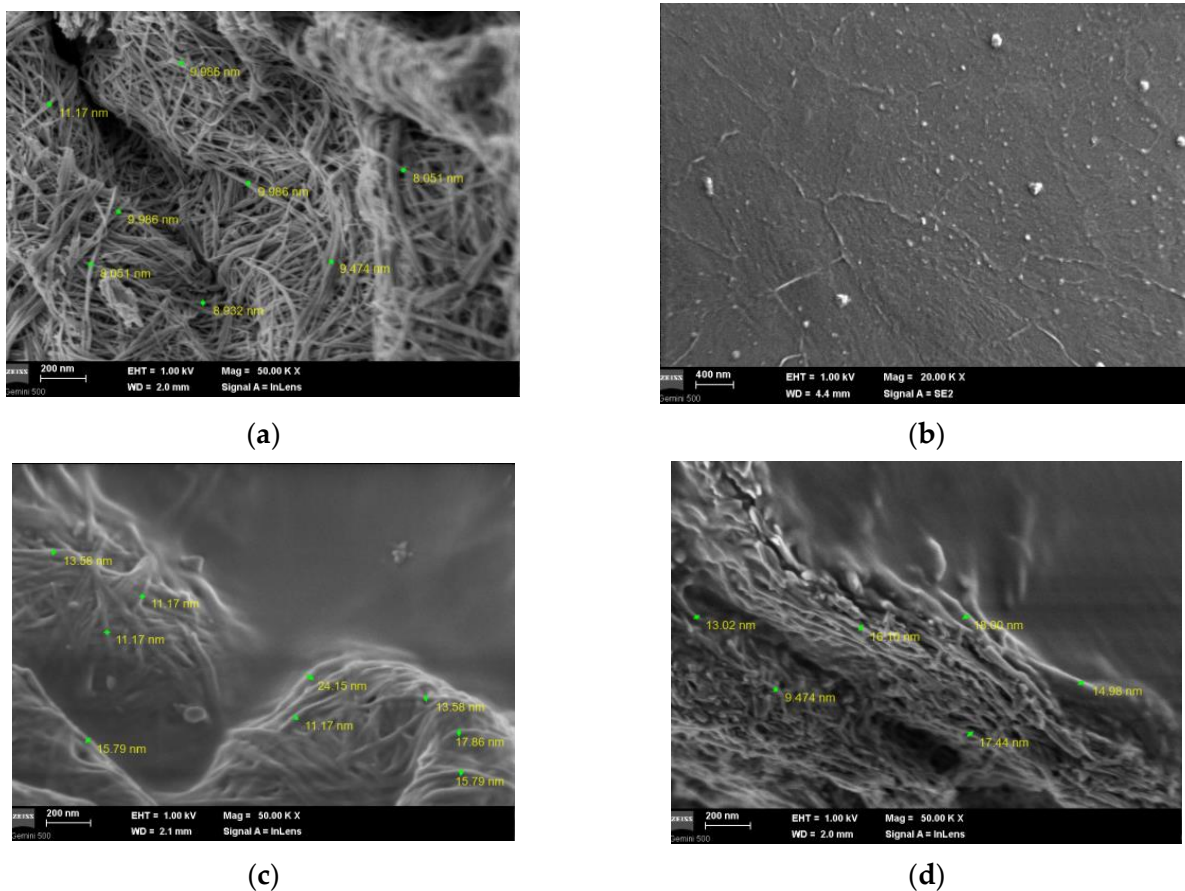


**Figure 2.** The SEM images of TiO<sub>2</sub> NWs (a), as well as TPU (b) and the TPU–TiO<sub>2</sub> NW composites, which have TiO<sub>2</sub> NW concentrations equal to 2 wt.% (c) and 17 wt.% (d), respectively.

According to Figure 2a, the TiO<sub>2</sub> NWs diameter varies between 8 and 11 nm. In contrast with Figure 2b, which shows an SEM image of TPU, in the case of Figure 2c,d, one can observe that the TPU–TiO<sub>2</sub> NW composites show a fibrous structure, while the TiO<sub>2</sub> NW diameter varies in the case of the TPU–TiO<sub>2</sub> NW composites that have TiO<sub>2</sub> NW concentrations of 2 wt.% and 17 wt.%, respectively, between 11 and 24 nm and 9 and 18 nm, respectively. The apparent increase in the diameter of TiO<sub>2</sub> NWs is caused by the adsorption of polymer on the surface of TiO<sub>2</sub> nanoparticles. Figure 3 shows the EDS spectra of TiO<sub>2</sub> NWs, as well as the TPU and the TPU–TiO<sub>2</sub> NW composites, which have a TiO<sub>2</sub> NW concentration equal to 2 wt.% (c) and 17 wt.%, respectively.



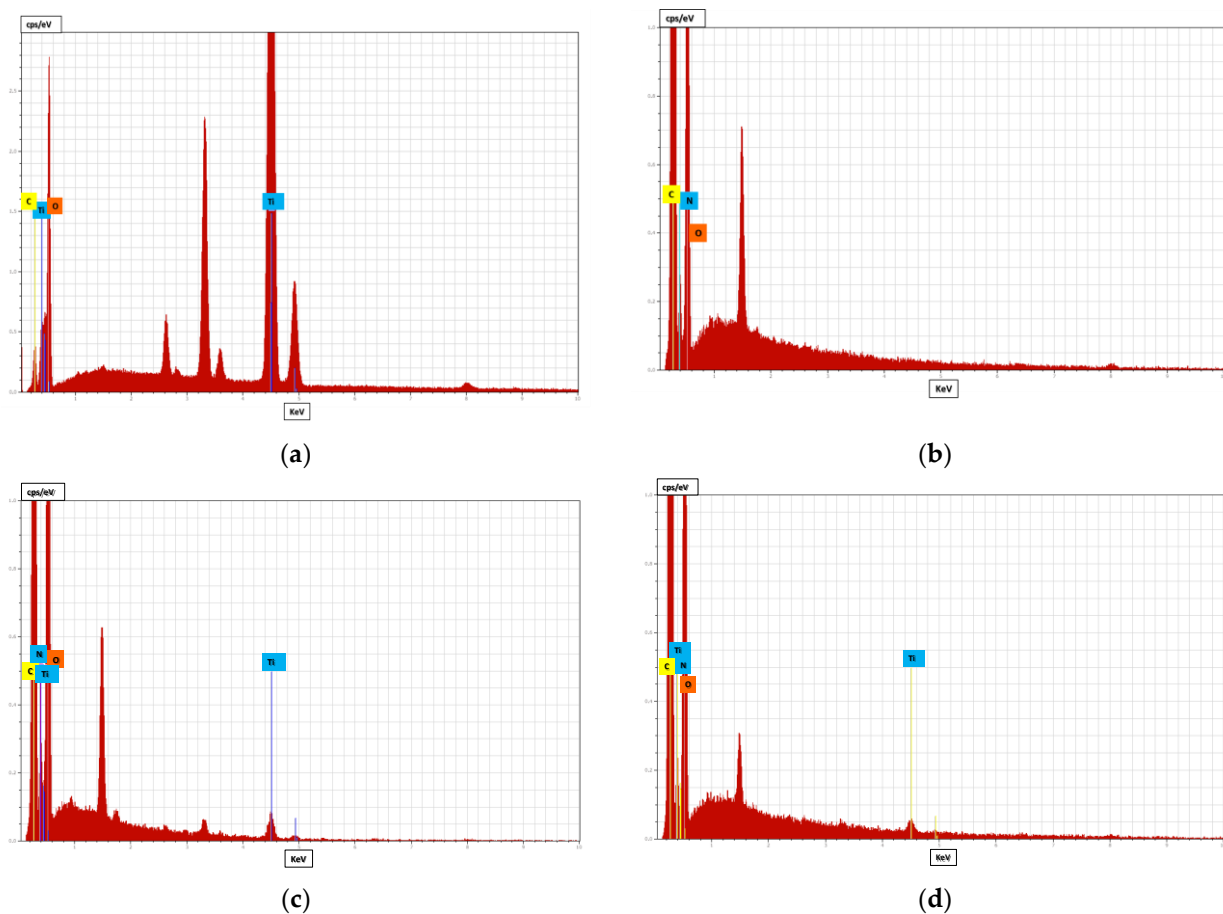


**Figure 3.** The EDS spectra of TiO<sub>2</sub> NWs (a), TPU (b) and the TPU–TiO<sub>2</sub> NW composites having the TiO<sub>2</sub> NW concentration equal to 2 wt.% (c) and 17 wt.% (d). The unassigned maxima belong to the sample fixation substrate.

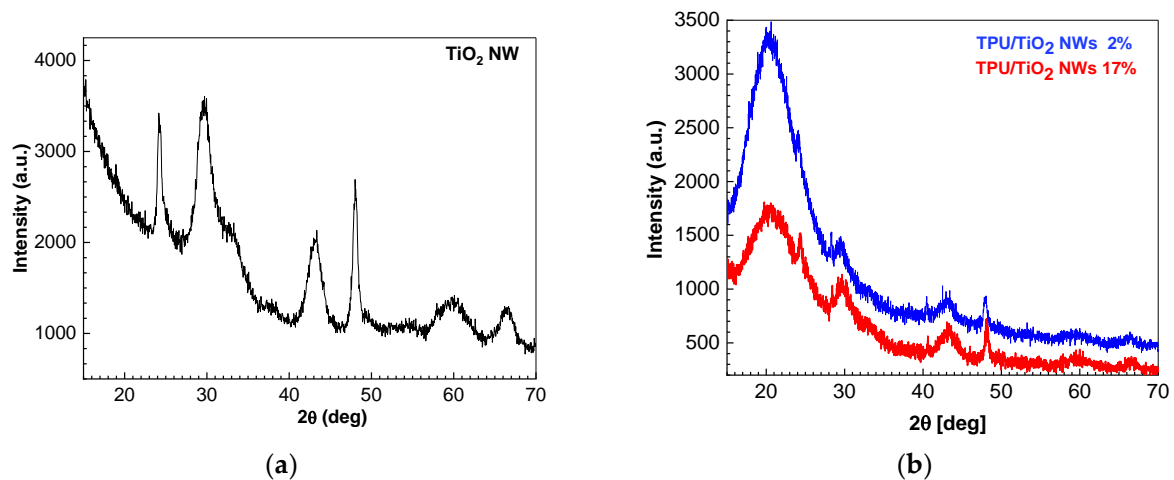
As we expected, Figure 3a,c,d proved the presence of Ti, which in the case of the TPU–TiO<sub>2</sub> NW composites confirms the embedding TiO<sub>2</sub> NWs in the TPU matrix, inducing a fibrous structure in the free-standing films.

### 3.2. Structural Properties of TiO<sub>2</sub> NWs and the TPU–TiO<sub>2</sub> Composites

Figure 4 shows the XRD patterns of TPU and the TPU–TiO<sub>2</sub> NW composites, which have TiO<sub>2</sub> NW concentrations equal to 2 wt.% and 17 wt.%, respectively. Figure 4a highlights the XRD patterns of TiO<sub>2</sub> NWs peak at 24.2°, 29.7°, 43.4°, 48°, 59.9°, and 66.5° in two theta. According to the standard International Centre for Diffraction Data (ICDD) database, the first two peaks situated at 24.2° and 29.7° belong to the crystalline (110) and (310) planes of the monoclinic (M) H<sub>2</sub>Ti<sub>3</sub>O<sub>7</sub> [44], PDF no.00-041-0192, while the peaks localized at 43.4° and 48° were assigned to the (200) plane in Ti<sub>0.91</sub>O, which has a cubic (C) crystalline structure [PDF no.04-004-2981], and the (200) plane in TiO<sub>2</sub> of the type tetragonal anatase (A) [45,46], PDF no. 00-021-1272, respectively. The peaks around 60.2° and 66.3° in 2θ belong to the (501) and (404) planes, respectively, of a Ti<sub>2</sub>O<sub>3</sub> phase with an orthorhombic (OR) crystalline structure (PDF04-018-9746).

Compared with Figure 4a, in the case of the TPU–TiO<sub>2</sub> NW composites with TiO<sub>2</sub> NW concentrations equal to 2 wt.% and 17 wt.%, one observes that: (i) the gradual increase in the added TiO<sub>2</sub> NWs is clearly visible at the NWs' specific 2θ angles; (ii) the peak in the range 15–25° (Figure 4b) belongs to TPU [43]; (iii) a shift in the peaks from 43.4° and 48° (Figure 4a) to 43.5° and 48.3° (blue curve in Figure 4b) or 43.6° and 48.1° (red curve in Figure 4b) occurs; and (iv) there is a change in the ratio between the intensities of the peaks at 43.4–43.6° and 48–48.3° from 0.78 (Figure 4a) to close to 1, i.e., 1.03 (blue curve in

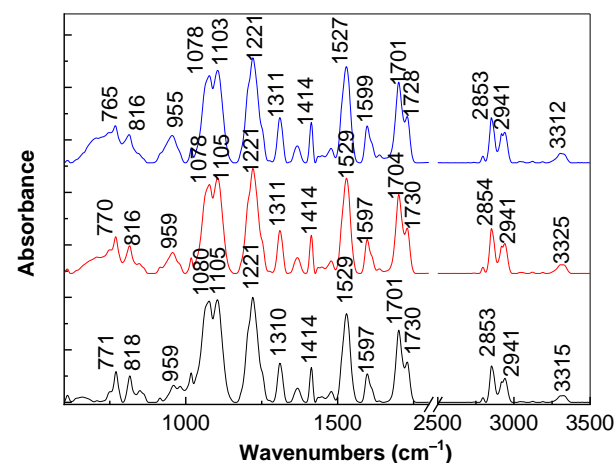
Figure 4b) and 0.96 (red curve in Figure 4b). This decrease in the intensity of the peak at  $48\text{--}48.3^\circ$  can only be explained if an interaction of  $\text{TiO}_2$  NWs with TPU occurs, when we estimate that the formation of suboxides takes place. To prove this claim, correlated Raman scattering and FTIR spectroscopy studies are presented below.



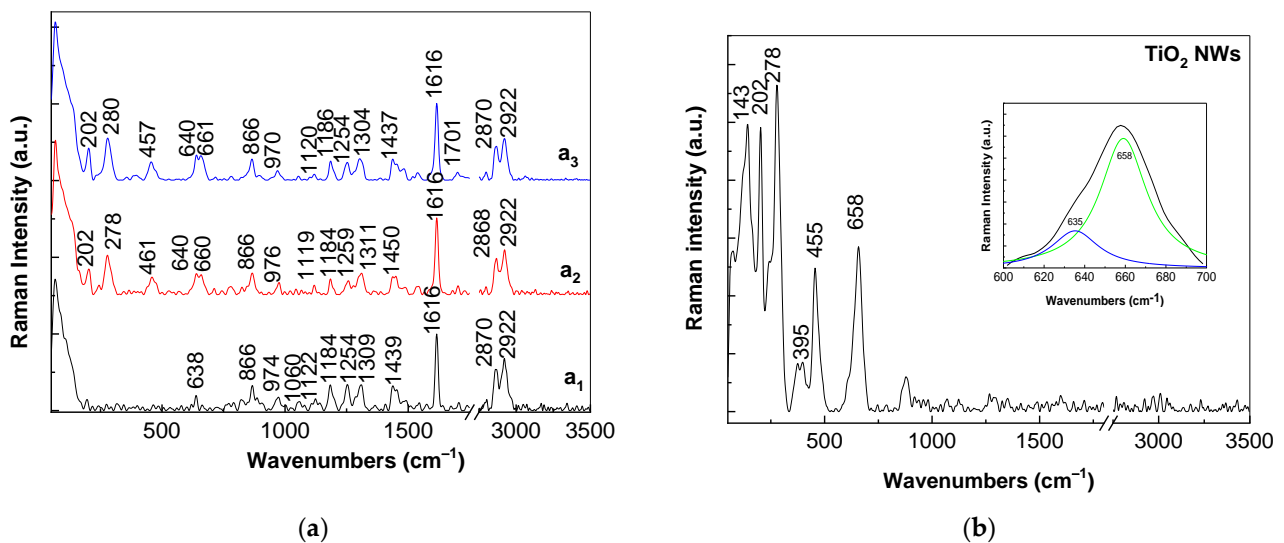
**Figure 4.** The XRD patterns of  $\text{TiO}_2$  NWs (a) and the TPU– $\text{TiO}_2$  NW composites (b) with  $\text{TiO}_2$  NW concentrations equal to 2 wt.% (blue curve in Figure 4b) and 17 wt.% (red curve in Figure 4b).

### 3.3. Vibrational Properties of TPU and the TPU– $\text{TiO}_2$ NW Composites

Figures 5 and 6 show the IR and Raman spectra of the TPU– $\text{TiO}_2$  NW composites with  $\text{TiO}_2$  NW concentrations equal to 2 wt.% and 17 wt.%. The main IR bands of TPU peaked at 771, 818, 959, 1080–1105, 1221, 1310, 1414, 1529, 1597, 1701, 1730, 2853–2941, and  $3315\text{ cm}^{-1}$  (Figure 5a). They are assigned to the vibrational modes of the N–H bond, C–H bond, higher-order aggregates, stretching C(O)–OC, CO stretching in the ether group, C–N bond, C–H bond, urethane group, C–C + C=C bonds in the benzene ring, hydrogen-linked urethane carbonyl group (C=O), the free carbonyl group, the antisymmetric and symmetrical vibrational modes of the CH bonds, and a partial inter- and intramolecular hydrogen linkage of the NH groups of the adjacent urethane segments [47–53], respectively.



**Figure 5.** IR spectra of TPU (a, black curve) and TPU– $\text{TiO}_2$  NW composites, which have  $\text{TiO}_2$  NW concentrations equal to 2 wt.% (b, red curve) and 17 wt.% (c, blue curve).



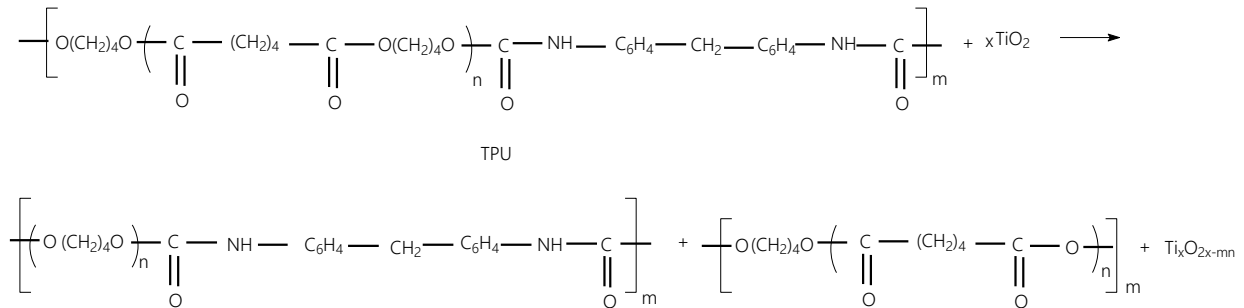
**Figure 6.** Raman spectra of: (a) TPU ( $a_1$ ); TPU–TiO<sub>2</sub> NW composites with TiO<sub>2</sub> NW concentrations equal to 2 wt.% ( $a_2$ ) and 17 wt.% ( $a_3$ ); and (b) TiO<sub>2</sub> NWs.

Figure 5 shows that as the TiO<sub>2</sub> NW concentration in the mass of the TPU–TiO<sub>2</sub> NW composites increases: (i) there is a shift of the IR band from 771 cm<sup>−1</sup> (Figure 5a) to 765 cm<sup>−1</sup> (Figure 5c); (ii) a shift of the IR band from 959 cm<sup>−1</sup> (Figure 5a) to 955 cm<sup>−1</sup> (Figure 5b,c), the variation accompanied by a decrease in the ratio between the absorbance of the IR bands from 771–765 and 955–959 cm<sup>−1</sup> from 1.82 (Figure 5a) to 1.75 (Figure 5b) and 1.32 (Figure 5c); (iii) a shift in the IR band from 3315 cm<sup>−1</sup> (Figure 5a) to 3304 cm<sup>−1</sup> (Figure 5c); and (iv) a variation in the ratio between the absorbance of the IR bands peaked at 765–771 cm<sup>−1</sup> and 3304–3315 cm<sup>−1</sup> from 4.68 (Figure 5a) to 4.21 (Figure 5b) and 3.83 (Figure 5c). These variations indicate a decrease in the higher-order aggregates of TPU simultaneous with the increase in the hydrogen bonds established between the amide groups of TPU and oxygen atoms of TiO<sub>2</sub> NWs.

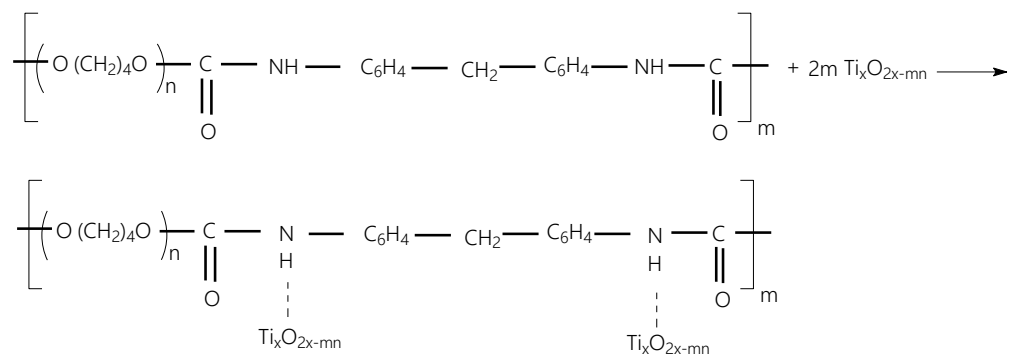
Additional information concerning the chemical structure of the TPU–TiO<sub>2</sub> NW composites is shown in Figure 6. The main Raman lines of TPU are situated at 638, 866, 974, 1060, 1122, 1184, 1254, 1309, 1439, 1616, and 2870–2922 cm<sup>−1</sup> (Figure 6a<sub>1</sub>), and they are assigned to the following vibrational modes: O–C=O in-plane deformation, out-of-plane benzene-ring deformation, out-of-plane C–H wagging, C–C skeletal stretching in alkane group, C–O–C, urethane amide, urethane amide III, deformation of the C–H bond in urethane amide III, symmetric stretching of N=C=O + deformation of CH<sub>2</sub> group, stretching of the bonds C–C + C=C in aryl ring, and stretching of CH bond in aromatic structure [54,55], respectively.

Figure 6b shows that the main Raman lines of TiO<sub>2</sub> NWs are localized at 143, 202, 278, 395, 455, and 658 cm<sup>−1</sup>, and they are assigned to the vibrational modes E<sub>g</sub> in TiO<sub>2</sub> A [56,57], stretching O–Ti–O in Ti<sub>2</sub>O<sub>3</sub> [58], O–Ti–O in Ti<sub>n</sub>O<sub>2n−1</sub> [58], B<sub>1g</sub> in TiO<sub>2</sub> A [56], A<sub>1g</sub> in H<sub>2</sub>Ti<sub>3</sub>O<sub>7</sub> [44], and E<sub>g</sub> in H<sub>2</sub>Ti<sub>3</sub>O<sub>7</sub>, respectively [44]. Increasing the concentration of TiO<sub>2</sub> NWs in the mass of the TPU–TiO<sub>2</sub> NW composites induces an increase in the intensity of the Raman lines peaking at 278–280 cm<sup>−1</sup>, an upshift of the Raman line from 455 cm<sup>−1</sup> (Figure 6b) to 457–461 cm<sup>−1</sup> (Figure 6a<sub>2,a3</sub>), and a change in the profile of the Raman line at 658 cm<sup>−1</sup> (Figure 6b). The insert in Figure 6b shows that the Raman line at 658 cm<sup>−1</sup> displays an asymmetric profile to small wavenumbers as a consequence of the presence of a Raman line peaked at 635 cm<sup>−1</sup>, belonging to the vibrational mode E<sub>g</sub> of H<sub>2</sub>Ti<sub>3</sub>O<sub>7</sub> [56]. Regarding the Raman spectra of TiO<sub>2</sub> NWs, the ratio between the intensity of the Raman lines peaked at 658 cm<sup>−1</sup> and 635 cm<sup>−1</sup>, which were assigned to the vibrational modes E<sub>g</sub> in TiO<sub>2</sub> A and E<sub>g</sub> in H<sub>2</sub>Ti<sub>3</sub>O<sub>7</sub> ( $I_{\text{TiO}_2\text{-A}}/I_{\text{H}_2\text{Ti}_3\text{O}_7}$ ), respectively, is equal to 3.45. Regarding the Raman spectra of the TPU–TiO<sub>2</sub> NW composites with the TiO<sub>2</sub> NW concentrations of 2 wt.% and 17 wt.%, the  $I_{\text{TiO}_2\text{-A}}/I_{\text{H}_2\text{Ti}_3\text{O}_7}$  ratio is equal to 0.94 (Figure 6a<sub>2</sub>) and 0.96 (Figure 6a<sub>3</sub>), respectively. The decrease in the value of the  $I_{\text{TiO}_2\text{-A}}/I_{\text{H}_2\text{Ti}_3\text{O}_7}$  ratio in the case

of the TPU–TiO<sub>2</sub> NW composites indicates a diminution of TiO<sub>2</sub> A in the TiO<sub>2</sub> NWs mass. This fact can be explained by taking into account the exchange reaction of TPU according to Scheme 1, which is followed by the formation of new hydrogen bonds between the NH bonds of the amide groups and the oxygen atoms of Ti<sub>x</sub>O<sub>2x-mn</sub> (Scheme 2).



**Scheme 1.** Exchange reaction of TPU in presence of TiO<sub>2</sub> NWs.



**Scheme 2.** Physical adsorption of polymer with repeating units containing amide groups onto Ti<sub>x</sub>O<sub>2x-mn</sub> surface.

The reaction products of Scheme 1 can be described as follows: (a) the first corresponds to a macromolecular compound with amide groups in the repeating units; (b) the second corresponds to a macromolecular compound characterized by the repeating units having acetate groups; and (c) the third corresponds to suboxide Ti<sub>x</sub>O<sub>2x-mn</sub>.

Similar to Scheme 2, new hydrogen bonds emerge between the -NH- bond of the TPU amide group and the oxygen atoms of Ti<sub>x</sub>O<sub>2x-mn</sub>. Such hydrogen bonds can be invoked to occur between the -NH- bonds of the TPU amide groups and the oxygen atoms of Ti<sub>2</sub>O<sub>3</sub> and Ti<sub>0.91</sub>O.

Summarizing these results, the exchange reaction presented in Scheme 1 is confirmed by the change in the ratio between the intensities of the peaks at 43.4–43.6° and 48–48.3° from 0.78 (Figure 4a) to close to 1, i.e., 1.03 (blue curve in Figure 4b) and 0.96 (red curve in Figure 4b), which indicates the emergence of suboxide Ti<sub>x</sub>O<sub>2x-mn</sub>, as well as the decrease in the ratio between the intensity of the Raman lines peaked at 658 cm<sup>-1</sup> and 635 cm<sup>-1</sup>, which is assigned to the vibrational modes E<sub>g</sub> in TiO<sub>2</sub> A and E<sub>g</sub> of H<sub>2</sub>Ti<sub>3</sub>O<sub>7</sub>, from 3.45 to 0.94–0.95 in the case of TPU and the TPU–TiO<sub>2</sub> NW composites (Figure 6). This indicates that there is a decrease in the higher-order aggregates as a consequence of the emergence of new hydrogen bonds between the -NH-, which belongs to the TPU amide groups, and the oxygen atoms of Ti<sub>x</sub>O<sub>2x-mn</sub>, Ti<sub>2</sub>O<sub>3</sub>, and Ti<sub>0.91</sub>O.

### 3.4. Photoluminescence of TPU and the TPU–TiO<sub>2</sub> NWs Composites

Figure 7 shows the PL spectra of TPU and the TPU–TiO<sub>2</sub> NW composites have a TiO<sub>2</sub> NW concentration equal to 2 wt.% and 17 wt.%. The increase in the TiO<sub>2</sub> NW concentration in the TPU–TiO<sub>2</sub> NW composites mass from 0 wt.% to 17 wt.% induces a shift in the maximum level of the emission band from 416 nm (Figure 7a<sub>1</sub>) to 457 nm



(Figure 7b<sub>1</sub>) and 480 nm (Figure 7c<sub>1</sub>), as well as a decrease in the intensity of the PL band from  $1.55 \times 10^7$  counts/sec (Figure 7a<sub>1</sub>) to  $2.76 \times 10^6$  counts/sec (Figure 7b<sub>1</sub>) and  $2.2 \times 10^6$  counts/sec (Figure 7c<sub>1</sub>). This decrease in the PL band indicates that TiO<sub>2</sub> NWs are PTU PL quenching agents. According to G. Strat et al., the redshift of the TPU's PL band results from the luminescence centers belonging the small-order aggregates [59], which in our case appear as a consequence of the reactions shown in Schemes 1 and 2.

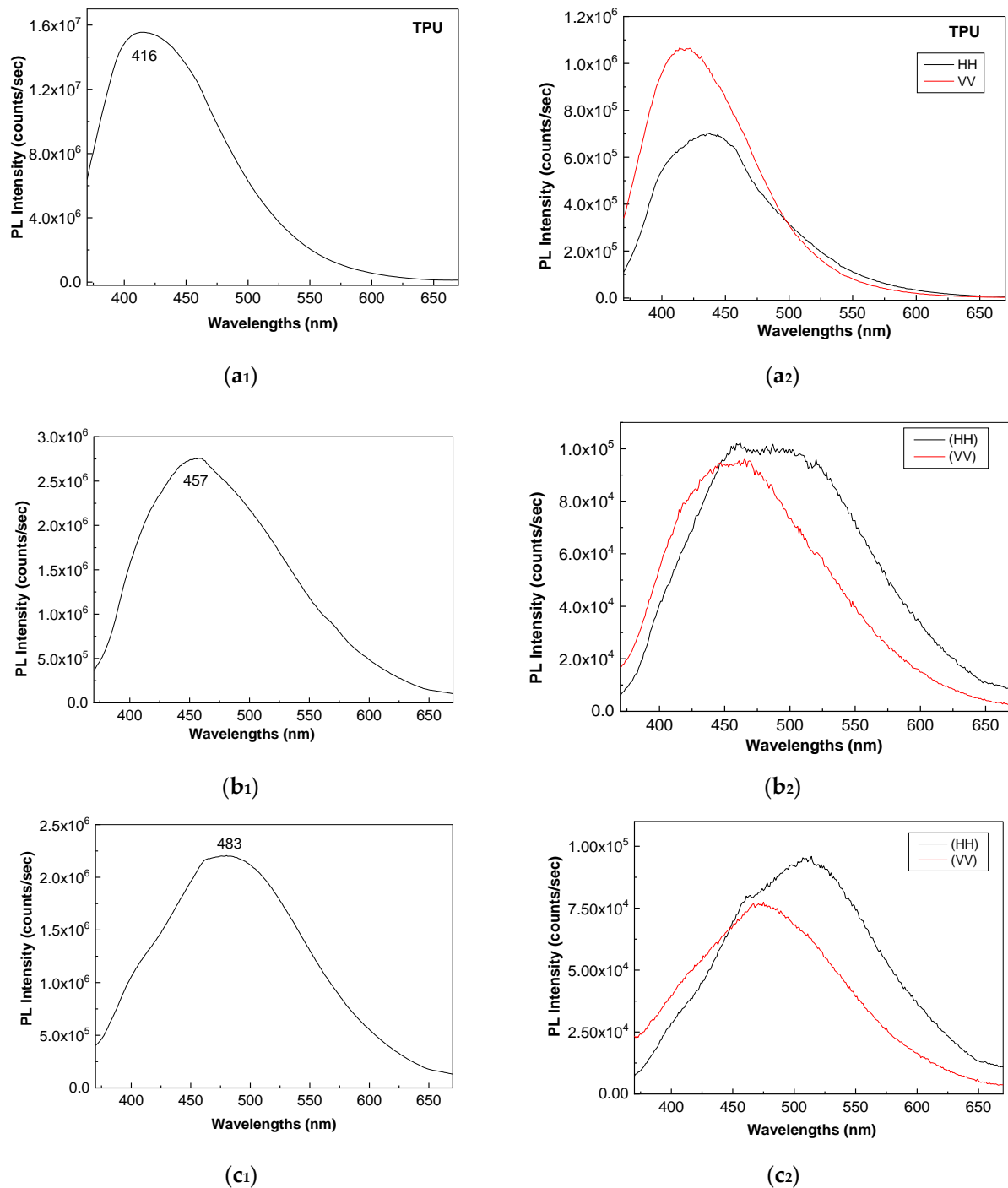


**Figure 7.** PL spectra of TPU (a<sub>1</sub>), PTU-TiO<sub>2</sub> NWs 2% (b<sub>1</sub>), and PTU-TiO<sub>2</sub> NWs 17% (c<sub>1</sub>). Anisotropic PL of TPU (a<sub>2</sub>), PTU-TiO<sub>2</sub> NWs 2% (b<sub>2</sub>), and PTU-TiO<sub>2</sub> NWs 17% (c<sub>2</sub>). In (a<sub>2</sub>, b<sub>2</sub>, c<sub>2</sub>), blue and red curves correspond to PL spectra recorded when measurement geometry for emission and excitation polarizers are both in horizontal (HH) and vertical (VV) position.

Using the mathematic protocol reported in [60], the calculated values of the anisotropy ( $r$ ) and binding angle ( $\theta_{PL}$ ) for TPU are 0.3712 and  $12.6^\circ$ , respectively, while the PTU–TiO<sub>2</sub> NW composite has a TiO<sub>2</sub> NW concentration equal to 2 wt.%, which is 0.2315 and  $32^\circ$ , and the PTU–TiO<sub>2</sub> NW composite has a TiO<sub>2</sub> NW concentration of 17 wt.%, which is 0.0905 and  $45.9^\circ$ . These values indicate that increasing the TiO<sub>2</sub> NW concentration in the PTU–TiO<sub>2</sub> NW composite mass results in an increase in  $\theta_{PL}$  of TPU onto the TiO<sub>2</sub> NW surface. As shown above, the  $\theta_{PL}$  values are different from  $0^\circ$ , which suggests that the TPU's excitation and emission transition dipoles are not parallel with the TiO<sub>2</sub> NW plane. The orientation of TPU onto the TiO<sub>2</sub> NW surface must consider the hydrogen bonds established between TiO<sub>2</sub> NWs and TPU as well as the products of TPU's exchange reaction with TiO<sub>2</sub> NWs.

#### 4. Conclusions

In this work, we reported new results concerning the optical and structural properties of TPU–TiO<sub>2</sub> NW composites as free-standing films. Our results highlight the following conclusions: (i) using X-ray diffraction, we demonstrated that TiO<sub>2</sub> NWs contain TiO<sub>2</sub> anatase (A), Ti<sub>0.91</sub>O and Ti<sub>2</sub>O<sub>3</sub> have cubic (C)- and orthorhombic (OR)-type crystalline structures, respectively, while H<sub>2</sub>Ti<sub>3</sub>O<sub>7</sub> has a monoclinic (M)-type structure; (ii) in the case of TPU–TiO<sub>2</sub> NW composites, with TiO<sub>2</sub> NW concentration 2 wt.% and 17 wt.%, the increase in the intensity of the diffraction peak localized at  $43.2^\circ$  indicated the formation of titanium suboxides; (iii) according to studies using FTIR spectroscopy, the interaction of TPU with TiO<sub>2</sub> NWs involved a decrease in the higher-order aggregates of TPU simultaneous with an increase in the hydrogen bonds established between the TPU amide groups and oxygen atoms of TiO<sub>2</sub> NWs, facts that were highlighted by the variation of the ratio between the absorbance of the IR bands peaking at  $765\text{--}771\text{ cm}^{-1}$  and  $3304\text{--}3315\text{ cm}^{-1}$  from 4.68 to 3.83 when the concentration of TiO<sub>2</sub> NWs in the composite mass was 0 wt.% and 17 wt.%; (iv) according to Raman spectroscopy, the decrease in the ratio between the intensity of the Raman lines peaked at  $658\text{ cm}^{-1}$  and  $635\text{ cm}^{-1}$ , which were assigned to the vibrational modes  $E_g$  in TiO<sub>2</sub> A and  $E_g$  in H<sub>2</sub>Ti<sub>3</sub>O<sub>7</sub> ( $I_{TiO_2-A}/I_{H_2Ti_3O_7}$ ), respectively, from 3.45 in TiO<sub>2</sub> NWs to 0.94–0.96 in the TPU–TiO<sub>2</sub> NW composites, indicating that the adsorption of TPU onto TiO<sub>2</sub> NWs involves an exchange reaction of TPU in the presence of TiO<sub>2</sub> NWs, which is followed by the formation of new hydrogen bonds between the -NH- of the amide group and the oxygen atoms of Ti<sub>x</sub>O<sub>2x-mn</sub>, Ti<sub>2</sub>O<sub>3</sub>, and Ti<sub>0.91</sub>O; (v) we demonstrated that the TiO<sub>2</sub> NWs are TPU PL quenching agents, which was evidenced by the decrease in the intensity of the emission band of the TPU–TiO<sub>2</sub> NW composite, which was localized in the spectral range 380–650 nm as increasing TiO<sub>2</sub> NW concentration; and (vi) anisotropic photoluminescence studies indicated a preferential orientation of TPU onto the TiO<sub>2</sub> NW surface, such as when increasing the TiO<sub>2</sub> NW concentration in the PTU–TiO<sub>2</sub> NW composite mass from 0 wt.% to 2 wt.% and 17 wt.%, which induced the increase in the polymer binding angle onto the TiO<sub>2</sub> NW surface ( $\theta_{PL}$ ) from  $12.6^\circ$  to  $32^\circ$  and  $45.9^\circ$ .

**Author Contributions:** Conceptualization, M.B. and R.C.; methodology, M.B.; investigation, M.S., T.B., M.P., A.L., E.M. and M.B.; writing—original draft preparation, M.B. and R.C.; writing—review and editing, M.B.; visualization, M.S., T.B., M.P., A.L., E.M. and R.C.; supervision, M.B.; funding acquisition, M.B. All authors have read and agreed to the published version of the manuscript.

**Funding:** This research was funded by the European Regional Development Fund under the Competitiveness Operational Program 2014–2020, financing contract 58/05.09.2016 (POC), type D subcontract 62/13.04.2022.

**Institutional Review Board Statement:** Not applicable.

**Informed Consent Statement:** Not applicable.

**Data Availability Statement:** The data reported in this manuscript are available upon request from the corresponding author.

**Acknowledgments:** This research was funded by the European Regional Development Fund under the Competitiveness Operational Program 2014–2020, financing contract 58/05.09.2016 (POC), type D subcontract of 62/13.04.2022.

**Conflicts of Interest:** The authors declare no conflict of interest. The funders had no role in the design of the study, collection, analyses, or interpretation of data, writing of the manuscript, or decision to publish the results.

## References

1. Wang, X.; Li, Z.; Shi, J.; Yu, Y. One-dimensional titanium dioxide nanomaterials: Nanowires, nanorods and nanobelts. *Chem. Rev.* **2014**, *114*, 9346–9384. [[CrossRef](#)] [[PubMed](#)]
2. Liu, Y.; Zhao, C.; Wang, X.; Xu, H.; Wang, H.; Zhao, X.; Feng, J.; Yan, W.; Ren, Z. Preparation of PPY/TiO<sub>2</sub> core-shell nanorods film and its photocathodic protection for 304 stainless steel under visible light. *Mat. Res. Bull.* **2020**, *124*, 110751. [[CrossRef](#)]
3. Sathasivam, K.; Wang, M.Y.; Anbalagan, A.K.; Lee, C.H.; Yeh, T.K. Prolonged and enhanced protection against corrosion over titanium oxide-coated 304L stainless steels having been irradiated with ultraviolet. *Front. Mater.* **2022**, *9*, 8630603. [[CrossRef](#)]
4. Gordon, T.R.; Cargnello, M.; Paik, T.; Mangolini, F.; Weber, R.T.; Fornasiero, P.; Murray, C.B. Nonaqueous synthesis of TiO<sub>2</sub> nanocrystals using TiFu to engineer morphology, oxygen, vacancy concentration, and photocatalytic activity. *J. Am. Chem. Soc.* **2012**, *134*, 6751–6761. [[CrossRef](#)]
5. Suprabha, T.; Roy, H.G.; Thomas, J.; Kumar, K.P.; Mathew, S. Microwave-assisted synthesis of titania nanocubes, nanospheres and nanorods for photocatalytic dye degradation. *Nanoscale Res. Lett.* **2009**, *4*, 144–154. [[CrossRef](#)]
6. Arami, H.; Mazloumi, M.; Khalifehzadeh, R.; Sadrnezhad, S.K. Sonochemical properties of TiO<sub>2</sub> nanoparticles. *Mat. Lett.* **2007**, *61*, 4559–4561. [[CrossRef](#)]
7. Raut, N.C.; Mathews, T.; Chandramohan, P.; Srinivasan, M.P.; Dash, S.; Tyagi, A.K. Effect of temperature on the growth of TiO<sub>2</sub> thin films synthesized by spray pyrolysis: Structural, compositional and optical properties. *Mat. Research. Bull.* **2011**, *46*, 2057–2063. [[CrossRef](#)]
8. Zhang, Z.Y.; Shao, C.; Li, X.H.; Sun, Y.Y.; Zhang, M.Y.; Mu, J.B.; Zhang, P.; Guo, Z.C.; Liu, Y.C. Hierarchical assembly of ultrathin hexagonal SnS<sub>2</sub> nanosheets onto electrospun TiO<sub>2</sub> nanofibers: Enhanced photocatalytic activity based on photoinduced interfacial charge transfer. *Nanoscale* **2013**, *5*, 606–618. [[CrossRef](#)]
9. Liu, W.; Tang, H.J.; Liu, D.Y. Combining density functional theory and CFD-PBM model to predict TiO<sub>2</sub> nanoparticle evolution during chemical vapor deposition. *Chem. Eng. J.* **2023**, *454*, 140174. [[CrossRef](#)]
10. Jain, N.; Zhu, Y.; Maurya, D.; Varghese, R.; Priya, S.; Hudait, M.K. Interfacial band alignment and structural properties of nanoscale TiO<sub>2</sub> thin films for integration with epitaxial crystallographic oriented germanium. *J. Appl. Phys.* **2014**, *115*, 024303. [[CrossRef](#)]
11. Aarik, J.; Aidla, A.; Sammelselg, V.; Uustare, T. Effect of growth conditions on formation of TiO<sub>2</sub>-II thin films in atomic layer deposition process. *J. Cryst. Growth* **1997**, *181*, 259–264. [[CrossRef](#)]
12. Zhou, X.H.; Zhou, X.F. Pulse laser deposition preparation and laser-induced voltage signals of TiO<sub>2</sub> thin films. *Thin Solid Films* **2022**, *756*, 139375. [[CrossRef](#)]
13. Lee, Y.H.; Yoo, J.M.; Park, D.H.; Kim, D.H.; Jee, B.K. Co-doped TiO<sub>2</sub> nanowire electric field-effect transistors fabricated by suspended molecular template method. *Appl. Phys. Lett.* **2005**, *86*, 033110. [[CrossRef](#)]
14. Li, M.; Luo, S.; Wu, P.; Shen, J. Photocathodic protection effect of TiO<sub>2</sub> films for carbon steel in 3% NaCl solutions. *Electrochim. Acta* **2005**, *50*, 3401–3406. [[CrossRef](#)]
15. Safajou, H.; Khojasteh, H.; Salavati-Niasari, M.; Mortazavi-Derazkola, S. Enhanced photocatalytic degradation of dyes over graphene/Pd/TiO<sub>2</sub> nanocomposites: TiO<sub>2</sub> nanowires versus TiO<sub>2</sub> nanoparticles. *J. Colloid. & Interface Sci.* **2017**, *498*, 423–432.
16. Zhou, X.M.; Liu, N.; Schmuki, P. Photocatalysis with TiO<sub>2</sub> nanotubes: “Colorful” reactivity and designing site-specific photocatalytic centers into TiO<sub>2</sub> nanotubes. *ACS Catal.* **2017**, *7*, 3210–3235. [[CrossRef](#)]
17. Esmat, M.; El-Hosainy, H.; Tahawy, R.; Jevasuwan, W.; Tsunoji, N.; Fukata, N.; Ide, Y. Nitrogen doping-mediated oxygen vacancies enhancing co-catalyst-free solar photocatalytic H<sub>2</sub> production activity in anatase TiO<sub>2</sub> nanosheet assembly. *Appl. Catal. B-Environ.* **2021**, *285*, 119755. [[CrossRef](#)]
18. Xiong, Z.G.; Zhao, X.S. Nitrogen-doped titanate-anatase core-shell nanobelts with exposed {101} anatase facets and enhanced visible light photocatalytic activity. *J. Am. Chem. Soc.* **2012**, *134*, 5754–5757. [[CrossRef](#)]
19. Vajda, K.; Saszet, K.; Kedves, E.Z.; Kasa, Z.; Danciu, V.; Baia, L.; Magyari, K.; Hernadi, K.; Kovacs, G.; Pap, Z. Shape-controlled agglomeration of TiO<sub>2</sub> nanoparticles. New insights on polycrystallinity vs. single crystals in photocatalysis. *Ceramics Int.* **2016**, *42*, 3077. [[CrossRef](#)]
20. Li, L.D.; Yan, J.Q.; Wang, T.; Zhao, Z.J.; Zhang, J.; Gong, J.L.; Guan, N.J. Sub-10 nm rutile titanium dioxide nanoparticles for efficient visible-light-driven photocatalytic hydrogen production. *Nature Commun.* **2015**, *6*, 5881. [[CrossRef](#)]
21. Kibasomba, P.M.; Dhlamini, S.; Maaza, M.; Liu, C.P.; Rashad, M.M.; Rayan, D.A.; Mwakikunga, B.W. Strain and grain size of TiO<sub>2</sub> nanoparticles from TEM, Raman spectroscopy and XRD.; The revisiting of the Williamson-Hall plot method. *Results Phys.* **2018**, *9*, 628–635. [[CrossRef](#)]

22. Ou, H.H.; Liao, C.H.; Lo, S.L. Determination of X-ray diffraction on the phase transformation of microwave-assisted titanate nanotubes during thermal treatment. *J. Nanomat.* **2010**, *837384*, 2010. [[CrossRef](#)]
23. Di Paola, A.; Bellardita, M.; Palmisano, L. Brookite, the least known TiO<sub>2</sub> photocatalyst. *Catalyst* **2013**, *3*, 36–73. [[CrossRef](#)]
24. Basavarajappa, P.S.; Patil, S.B.; Ganganappa, N.; Reddy, K.R.; Raghu, A.V.; Reddy, C.V. Recent progress in metal-doped TiO<sub>2</sub>, non-metal doped/co-doped TiO<sub>2</sub> and TiO<sub>2</sub> nanostructured hybrids for enhanced photocatalysis. *Int. J. Hydrog. Energy* **2020**, *45*, 7764–7778. [[CrossRef](#)]
25. Arthi, R.; Jaikumar, V.; Muralidharan, P. Comparative performance analysis of electrospun TiO<sub>2</sub> embedded poly(vinylidene fluoride) nanocomposite membrane for supercapacitors. *J. Appl. Polym. Sci.* **2020**, *138*, e50323. [[CrossRef](#)]
26. Matysia, W.; Tanski, T.; Jarka, P.; Nowak, M.; Kepinska, M.; Szperlich, P. Comparison of optical materials of PAN/TiO<sub>2</sub>, PAN/Bi<sub>2</sub>O<sub>3</sub>, and PAN/SbSI nanofibers. *Opt. Mater.* **2018**, *83*, 145–151. [[CrossRef](#)]
27. Al-Mokaram, A.M.A.A.; Yahya, R.; Abdi, M.M.; Mahmud, H.N.M.E. The development of non-enzymatic glucose biosensors based on electrochemically prepared polypyrrole-chitosan-titanium dioxide nanocomposite films. *Nanomaterials* **2017**, *7*, 129. [[CrossRef](#)]
28. Wang, G.J.; Huang, X.J.; Jiang, P.K. Mussel-inspired fluoro-polydopamine functionalization of titanium dioxide nanowires for polymer nanocomposites with significantly enhanced energy storage capability. *Sci. Rep.* **2017**, *7*, 43071. [[CrossRef](#)]
29. Behniafar, H.; Yazdi, M.; Saki, F. Chemical preparation and characterization of fibrous poly(3-methyl thiophene) decorated by TiO<sub>2</sub> nanoparticles. *Int. J. Polym. Anal. Charact.* **2016**, *21*, 584–589. [[CrossRef](#)]
30. Chiang, C.J.; Lee, Y.H.; Lee, Y.P.; Lin, G.T.; Yang, M.H.; Wang, L.; Hsieh, C.C.; Dai, C.A. One-step in situ hydrothermal fabrication of D/A poly(3-hexyl thiophene)/TiO<sub>2</sub> hybrid nanowires and its application in photovoltaic devices. *J. Mater. Chem. A* **2016**, *4*, 908–919. [[CrossRef](#)]
31. Siuzdak, P.; Sawczak, M.; Lisowska-Oleksiak, A. Fabrication and properties of electrode materials composed of order titanium nanotubes and PEDOT:PSS. *Solid State Ionics* **2015**, *271*, 56–62. [[CrossRef](#)]
32. Guo, Y.N.; He, D.L.; Xia, S.B.; Xie, X.; Gao, X.; Zhang, Q. Preparation of a novel nanocomposite of polyaniline core decorated with anatase-TiO<sub>2</sub> nanoparticles in ionic liquid/water microemulsion. *J. Nanomater.* **2012**, *2012*, 202794. [[CrossRef](#)]
33. Glouia, Y.; Dhorib, S.; Abid, K. A comparative study of the effect of clay and titanium dioxide on the mechanical properties and permeability of nanocoated cotton fabrics. *J. Appl. Polym. Sci.* **2017**, *135*, 45642. [[CrossRef](#)]
34. Jian, Y.; Li, F.; Mei, Y.; Ding, Y.; Pang, H.; Zhang, P. Gel polymer electrolyte based on hydrophilic-lipophilic TiO<sub>2</sub>-modified thermoplastic polyurethane for high-performance Li-ion batteries. *J. Mater. Sci.* **2021**, *56*, 2474–2485. [[CrossRef](#)]
35. Ji, H.; He, D.; Li, B.; Lu, G.; Wang, C. Evaluation of rheological and anti-aging properties of TPU/nano-TiO<sub>2</sub> composite-modified asphalt binder. *Materials* **2022**, *15*, 3000. [[CrossRef](#)]
36. Simsek, R.; Polat, Y.; Pampal, E.S.; Agna, O.; Kibic, A. Ultrasonic coating of nanofibrous webs: A feasible approach to photocatalytic water filters. *J. Coat. Technol. Res.* **2016**, *13*, 89–95. [[CrossRef](#)]
37. Wei, O.; Oribayo, O.; Feng, X.; Remple, G.L.; Pan, Q. Synthesis of polyurethane foams loaded with TiO<sub>2</sub> nanoparticles and their modifications for enhanced performance in oil spill cleanup. *Ind. Eng. Chem. Res.* **2018**, *57*, 8918–8926. [[CrossRef](#)]
38. Zhang, J.; Li, X.; Guo, J.; Zhou, G.; Xiang, L.; Wang, X.; He, Z. Novel TiO<sub>2</sub>/TPU composite fiber-based smart textiles for photocatalytic applications. *Mater. Adv.* **2022**, *3*, 1518. [[CrossRef](#)]
39. Chen, X.; Wang, W.; Li, S.; Qian, Y.; Jiao, C. Synthesis of TPU/TiO<sub>2</sub> nanocomposites by molten blending method. *J. Therm. Anal. Calorim.* **2018**, *132*, 793–803. [[CrossRef](#)]
40. Rehman, W.U.; Rasheed, T.; Naveed, A.; Ali, A. Thermoplastic polyurethane/rutile titanium dioxide composites turned for hydrophobicity with effective reinforcement. *J. Polym. Res.* **2022**, *29*, 188. [[CrossRef](#)]
41. Suresh, S.; Black, R.A. Electrospun polyurethane as an alternative ventricular catheter and in vitro model of shunt obstruction. *J. Biomat. Appl.* **2015**, *29*, 1028–1038. [[CrossRef](#)]
42. Harris, C.A.; Resau, J.H.; Hedson, E.A. Effects of surface wettability, flow and protein concentration on macrophage and astrocyte adhesion in an in vitro model of central nervous system catheter obstruction. *J. Biomed. Mater. Res. Part A* **2011**, *97*, 433–440. [[CrossRef](#)] [[PubMed](#)]
43. Baibarac, M.; Nila, A.; Smaranda, I.; Stroe, M.; Stingescu, L.; Cristea, M.; Cercel, R.C.; Lorinczi, A.; Ganea, P.; Mercioniu, I.; et al. Optical, structural and dielectric properties of composites based on thermoplastic polymers of the polyolefin and polyurethane type and BaTiO<sub>3</sub> nanoparticles. *Materials* **2021**, *14*, 753. [[CrossRef](#)] [[PubMed](#)]
44. Garcia-Contreras, L.A.; Flores-Flores, J.O.; Arenas-Alatorre, J.A.; Chavez-Carvayar, J.A. Synthesis, characterization and study of the structural change of nanobelts of TiO<sub>2</sub> (H<sub>2</sub>Ti<sub>3</sub>O<sub>7</sub>) to nanobelts with anatase, brookite and rutile phases. *J. Alloys Compd.* **2022**, *923*, 166236. [[CrossRef](#)]
45. Li, W.; Liang, R.; Hu, A.; Huang, Z.; Zhou, Y.N. Generation of oxygen vacancies in visible light activated one-dimensional iodine TiO<sub>2</sub> photocatalysts. *RSC Adv.* **2014**, *4*, 36959. [[CrossRef](#)]
46. Sofyan, N.; Ridhova, A.; Yuwono, A.H.; Udhiarto, A. Preparation of anatase TiO<sub>2</sub> nanoparticles using low hydrothermal temperature for dye-sensitized solar cell. *IOP Conf. Ser. Mater. Sci. Eng.* **2018**, *316*, 012055. [[CrossRef](#)]
47. Ferry, A.; Jacobsson, P.; Van Heumen, J.; Stevens, J. Raman, infra-red and d.s.c. studies of lithium coordination in a thermoplastic polyurethane. *Polymer* **1996**, *37*, 737–744. [[CrossRef](#)]

48. Pattamaprom, C.; Wu, C.H.; Chen, P.H.; Huang, Y.L.; Raganathan, P.; Rwei, S.R.; Chuan, F.S. Solvent-free one-shot synthesis of thermoplastic polyurethane based in bio-poly(1, 3-propylene succinate)glycol with temperature-sensitive shape memory behavior. *ACS Omega* **2020**, *5*, 4058–4066. [[CrossRef](#)]
49. Sen, F.; Basturk, E.; Karadogan, B.; Madakbas, S.; Kahraman, M.V. Effect of barium titanate in the thermal, morphology, surface and mechanical properties of the thermoplastic polyurethane/barium titanate composites. *Polym. Plast. Technol. Eng.* **2016**, *55*, 1325–1331. [[CrossRef](#)]
50. Sarabiyan Nejad, S.; Babaie, A.; Bagheri, M.; Rezaei, M.; Abbasi, F.; Shomali, A. Effects of graphene quantum dot (GQD) on photoluminescence, mechanical, thermal and sharp memory properties of thermoplastic polyurethane nanocomposites. *Polym. Adv. Technol.* **2020**, *31*, 2279–2289.
51. Ning, L.; De-Ning, W.; Sheng-Kang, Y. Crystallinity and hydrogen bonding of hard segments in segmented poly(urethane urea) copolymers. *Polymer* **1996**, *37*, 3577–3583. [[CrossRef](#)]
52. Mattia, J.; Painter, P. A comparison of hydrogen bonding and other in a polyurethane and poly(urethane-urea) and their blends with poly(ethylene glycol). *Macromolecules* **2007**, *40*, 1546–1554. [[CrossRef](#)]
53. Allen, N.S.; McKellar, J.F. Photochemical reactions in an MDI-based elastomeric polyurethane. *J. Appl. Polym. Sci.* **1976**, *20*, 1441–1447. [[CrossRef](#)]
54. Parnell, S.; Min, K.; Cakmak, M. Kinetic studies of polyurethane polymerization with Raman spectroscopy. *Polymer* **2003**, *44*, 5137–5144. [[CrossRef](#)]
55. Lin-Vien, D.; Colthup, N.; Fateley, W.; Grasselli, J. *The Handbook of Infrared and Raman Characteristic Frequencies of Organic Molecules*, 1st ed.; Academic Press: San Diego, CA, USA, 1991.
56. Choi, H.C.; Jung, Y.M.; Kim, S.B. Size effects in the Raman spectra of TiO<sub>2</sub> nanoparticles. *Vib. Spectrosc.* **2005**, *37*, 33–38. [[CrossRef](#)]
57. Challagulla, S.; Tarafder, K.; Ganesan, R.; Roy, S. Structure sensitive photocatalytic reduction of nitroarenes over TiO<sub>2</sub>. *Sci. Rep.* **2017**, *7*, 8783. [[CrossRef](#)]
58. Chen, Y.; Mao, J. Sol-gel preparation and characterization of black titanium oxides Ti<sub>2</sub>O<sub>3</sub> and Ti<sub>3</sub>O<sub>5</sub>. *J. Mater. Sci. Mater. Electron.* **2014**, *25*, 1284–1288. [[CrossRef](#)]
59. Strat, G.; Buruiana, E.; Buruiana, T.; Pohoata, V.; Strat, M. Fluorescence properties of the polyurethane with anchored stilbene chromophore. *J. Optoelectr. Adv. Mater.* **2005**, *7*, 925–928.
60. Baibarac, M.; Ilie, M.; Baltog, I.; Lefrant, S.; Humbert, B. Infrared dichroism studies and anisotropic photoluminescence properties of poly(para-phenylene vinylene) functionalized reduced graphene. *RSC Adv.* **2017**, *7*, 6931–6942. [[CrossRef](#)]

**Disclaimer/Publisher's Note:** The statements, opinions and data contained in all publications are solely those of the individual author(s) and contributor(s) and not of MDPI and/or the editor(s). MDPI and/or the editor(s) disclaim responsibility for any injury to people or property resulting from any ideas, methods, instructions or products referred to in the content.